First-principles study of the stability of calcium-decorated carbon nanostructures

C. Cazorla,[*] S. A. Shevlin, and Z. X. Guo

Department of Chemistry, University College London, London WC1H 0AH, United Kingdom
and London Centre for the Theory and Simulation of Materials, London WC1E 6BT, United Kingdom
(Received 29 June 2010; revised manuscript received 4 October 2010; published 28 October 2010)

In view of the interest in calcium-decorated carbon nanostructures motivated by potential biotechnological and nanotechnological applications, we have carried out a systematic and thorough first-principles computational study of the energetic and structural properties of these systems. We use density-functional theory (DFT) and *ab initio* molecular dynamic simulations to determine minimum energy configurations, binding energy profiles and the thermodynamic stability of Ca-decorated graphene and carbon nanotubes (CNT) as function of doping concentration. In graphene, we predict the existence of an equilibrium $(\sqrt{3} \times \sqrt{3})$ R30° commensurate CaC_6 monolayer that remains stable without clustering at low and room temperatures. For carbon nanotubes, we demonstrate that uniformly Ca-decorated zigzag $(n \le 10,0)$ CNT become stable against clustering at moderately large doping concentrations while Ca-coated armchair (n,n) CNT exhibit a clear thermodynamic tendency for Ca aggregation. In both Ca-doped graphene and CNT systems, we estimate large energy barriers (∼1 eV) for atomic aggregation processes, which indicates that Ca clustering in carbon nanosurfaces may be kinematically hindered. Finally, we demonstrate via comparison of DFT and Møller-Plesset second-order perturbation calculations that DFT underestimates significantly the weak interaction between a Ca dopant and a coronene molecule, and also that the Ca-coronene system is not physically comparable to Ca-doped graphene due to lack of electronic π-d orbitals hybridization near the Fermi energy level.

I. INTRODUCTION

Functionalized carbon nanostructures (CNS) (e.g., graphene, fullerenes, and nanotubes)[1–6] show promise as applications in a number of scientific fields such as biomedicine, nanotechnology, energy materials, and catalysis. In recent years, functionalized carbon nanostructures have proved successful as drug delivery nanodevices, molecular sensors, actuators and integrated electronic components; also, there is considerable expectancy on using them in hydrogen fuel cell applications that could mitigate atmospheric green-house gas emissions produced by the burning of fossil fuels.[7–17]

A customary technique used for functionalization of carbon nanostructures consists in atomic doping of their surface and/or interior. Among all the chemical species, transition metals (TM) have attracted much attention because they bind quite strongly to nanomaterials and may enhance significantly their reactivity properties.[16,18–20] However, TM atoms tend to form clusters rather than to stay dispersed on the carbon surfaces due to the fact that typical TM cohesive bulk energies (∼−10 eV/atom) are much lower than those involved in TM-carbon nanostructure binding (∼−1 eV/atom).[21,22] This propensity for aggregation reduces gas-adsorption capacities of carbon-based nanomaterials severely, causing in some cases even unwanted molecular dissociation, thus it poses a major technical drawback in the development of novel gas storage applications.

Recently, alkali earth metals (AEM) have been proposed as a promising alternative to TM for achievement of reactive and stable nanostructure coatings.[23] In fact, typical cohesive energies of bulk AEM materials are in the range $-2 \le E_{coh} \le -1$ eV/atom and turn out to be comparable to the binding energy of isolated AEM atoms adsorbed on carbon surfaces (therefore, AEM tendency for atomic aggregation is expected to be rather small if not null). It is worth noting that calcium-decorated carbon nanostructures have already been predicted as high-capacity hydrogen storage nanomaterials[23–28] and they have been shown to interact attractively with small molecules such as dioxin[29] and simple amino acids composing the collagen protein.[30] Nevertheless, the issue about the stability of AEM-decorated carbon nanostructures has not been addressed satisfactorily to date as witnessed by the fact that the information reported on this topic so far appears to be confusing and in some cases even contradictory.

A few of years ago, Yoon *et al.*[23] were the first to study AEM-doped carbon nanostructures as potential high-capacity nanomaterials for hydrogen storage. Using first-principles energy-band calculations, they demonstrated that C_{60} fullerenes uniformly coated with Ca and Sr atoms can be stabilized via a peculiar bonding mechanism consisting of a charge donation from the $4s$ $(5s)$ Ca (Sr) orbitals to the fullerene π^* bands, and posterior charge back donation to the unoccupied $3d$ $(4d)$ Ca (Sr) orbitals. In the case of Mg and Be coatings, this stabilization does not occur because of the lack of hybridization between AEM d orbitals and fullerene π^* bands. In fact, C_{60} fullerene structures coated with uniform Ca monolayer have been obtained experimentally[31] so Yoon's predictions appear to be consistent with observations. Nevertheless, it has been recently suggested by Yang *et al.*[24] that uniformly Ca-coated C_{60} fullerenes must be considered as metastable since the binding energy of Ca adsorbates (−1.20 eV/atom, as reported in Ref. 24) turns out to be larger than the cohesive energy of bulk fcc Ca (−1.70 eV/atom, as reported by Yang *et al.*). Motivated by Yoon's results, Ataca *et al.* have conducted similar first-principles investigations on AEM-functionalized graphene.[25] The conclusions drawn by these authors are equivalent to those found for AEM-doped fullerenes, namely, that Ca and Sr atoms can form stable and uniform monolayers on top of

graphene while Be and Mg atoms do not. Analogous donation/back-donation electronic processes originally investigated in fullerenes have been found to occur also in AEM-coated graphene. Ataca *et al.*, however, note that despite clustering of AEM atoms being energetically slightly more favorable than graphene coating, this tendency is effectively hindered by repulsive Coulomb Ca-Ca interactions that result from substantial electronic charge transfers to the carbon surface. Kim *et al.*[32] have shown that structural defects like vacancies may further enhance the binding of Ca and Mg atoms, and then their dispersion, in graphene. With regard to AEM-decorated carbon nanotubes (CNT), so far only two different research groups have explored these systems using *ab initio* energy-band methods (not considering the present work). Lee *et al.*[26,27] have analyzed the stability of Ca-dispersed atoms adsorbed on armchair (n,n) nanotubes and graphene-based nanostructures and concluded that these systems are energetically unstable with respect to AEM clustering; in order to further enhance the stability of these systems the authors have proposed a lucid strategy based on mixed calcium-boron doping. Strikingly, Lee *et al.*[27] make the general statement that uniform and stable AEM coatings exist only for zigzag graphene nanoribbons, neither for carbon nanotubes nor for graphene, so apparently contradicting Yoon's and Ataca's work performed with equivalent computational approaches. In addition to that, Yang *et al.*[24] have demonstrated that uniform Ca adsorbates on zigzag $(4 \leq n \leq 7,0)$ nanotubes can be considered as stable since the corresponding binding energies lie below the cohesive energy of bulk Ca.

Most of the discrepancies about the stability of AEM-decorated nanostructures summarized here can be explained in terms of the definition of "clustering" and the method for evaluation of stability used by the different research groups. For instance, in Refs. 26 and 27 clustering is used as synonym for atoms to densely accommodate upon adsorption, however, in Ref. 23 the same term is used to express that nucleation of three-dimensional structures is energetically more favorable than formation of two-dimensional layers. In this work, clustering or "aggregation" terms will express AEM tendency to form three-dimensional structures rather than two-dimensional coatings (that is, in the same spirit as Yoon's definition). Consequently, if AEM atoms adhere to the carbon nanosurfaces closely one to the other but essential monolayer features remain preserved, we will not be talking about clustering.

Regarding the stability of generic A-decorated nanostructures, this is customarily evaluated by calculating first the binding energy E_{bind} of one or few A atoms dispersed on the carbon surfaces, and then comparing it with the cohesive energy of the corresponding pure A bulk material E_{coh}. If $E_{coh} \leq E_{bind}$, it is generally concluded that formation of clusters rather than uniform A-coating will occur, whether if $E_{bind} \leq E_{coh}$, the opposite aggregation behavior is assumed. In fact, this criterion appears to be valid in TM systems, where E_{coh} values are much smaller than E_{bind} values, however, it is not clear whether such a rule also applies correctly to AEM for the reasons that we explain next. First, the cohesive energy of a bulk material generally is much smaller than that of clusters (as we will illustrate later), so in prin-

ciple the tendency for aggregation on a surface can be practically null if the energy difference $\Delta E = E_{bind} - E_{coh}$ is positive but rather small (that is, of order ~ 0.1 eV as we will justify later). Second, binding energies generally depend on the number of atoms adsorbed on the surfaces so systematic studies on the effects of coverage must be carried out first before arriving at any conclusion. And third, even in the case that $E_{coh} \leq E_{bind}$ results after considering the previous points made, large energy barriers may exist that impede the formation of clusters in practice (that is, systems can be kinetically stable), so kinetic effects must be assessed.

In view of the recent expectations raised by Ca-decorated nanostructures in technology fields and due to the lack of clear consensus on their stability properties, we have conducted a systematic first-principles simulation study of Ca-adsorbates on graphene and carbon nanotubes (zigzag and armchair types) at low and ambient temperatures. In parallel, we also analyzed magnesium-coated nanostructures because these systems exhibit clear tendency for doping aggregation hence can be used to provide insightful comparisons. Our computational approach is based on density-functional theory (DFT) and three different types of calculations, namely, (i) binding energy as a function of AEM-coverage, (ii) *ab initio* molecular dynamic (AIMD) simulations, and (iii) transition energy barriers for atomic diffusion and AEM-dimer formation on top of carbon surfaces. Our calculations show that uniformly Ca-decorated nanostructures are most stable at moderately large Ca concentrations and that minimum energy structures found in graphene and zigzag CNTs are stable against clustering at ambient temperature.

The remainder of this article is as follows; in the next section, we explain the details of the computational methods and value of the technical parameters used in our calculations. In the same section, we report the results of a test in which we compare the performance of DFT and the more intricate and accurate Møller-Plesset second-order perturbation theory (MP2) method at describing metal cation-π interactions. Then, we present the results in Sec. III and finalize with a discussion and summary of the findings in Sec. IV.

II. COMPUTATIONAL OUTLINE AND TEST OF THE METHOD

Most of the calculations were performed using the projector augmented wave version of DFT as implemented in the VASP package.[33,34] Electronic orbitals $2s2p$, $3p4s$ and $2p3s$ were considered as valence states for C, Ca, and Mg atoms, respectively. We used the Perdew-Burke-Ernzerhof (PBE) form of generalized gradient approximation (GGA) to the exchange-correlation functional.[35] An energy cut-off of 400 eV was employed throughout and dense Monkhorst-Pack **k**-point grids[36] for electronic sampling were selected in order to guarantee convergence of the total energy to less than 1 meV/atom. Atomic forces in the geometry optimizations were required to amount to less than 0.01 eV/Å. A tolerance of 10^{-5} eV for the self-consistent loops and Fermi-Dirac smearing equivalent to an electronic temperature of 2000 K, were imposed. We performed charge-density distribution (CDD) analysis in some of the geometry optimized structures found based on the Bader theory.[37,38]

Binding energies per AEM atom were calculated using the formula

$$E_{bind}(N) = 1/N \cdot [E_{\text{system}} - (E_{\text{CNS}} + N \cdot E_{\text{AEM}})], \qquad (1)$$

where it is stressed that E_{bind} depends on the number of AEM atoms adsorbed on the CNS, N, E_{system} is the total energy of the geometry optimized AEM-doped nanomaterial, E_{CNS} is the energy of the relaxed carbon structure, and E_{AEM} the energy of one isolated AEM atom. According to this definition, and completely ignoring thermal and/or AEM aggregation effects, negative E_{bind} values indicate that AEM binding is thermodynamically favorable. Full atomic geometry relaxations were carried out using a conjugate-gradient algorithm that keeps the volume of the unit cell fixed and allows for variation in its shape.

At a given doping concentration, systematic AEM atomic arrangements were considered in one face of the graphene sheet or outer CNT surface. Typical size of the systems was 32 C atoms for graphene and 24 C $\leq N_{\text{CNT}} \leq 120$ C atoms for carbon nanotubes depending on CNT radius and chirality.

The study of the minimum energy path for atomic AEM diffusion and dimer formation processes on top of graphene and CNT was undertaken using the nudged elastic band (NEB) method.[39,40] By AEM-dimer formation we mean the process by which one of two AEM atoms, both initially adhered to the carbon surface and close one to the other, leaves the carbon surface to bind on top of its neighbor, which remains adsorbed, to form a dimer. This simple process is far from reproducing a full two-dimensional layer →three-dimensional structural phase transformation, however, it provides an approximate order of magnitude for the transition energy barriers involved. A total of 9 and 5 spring images were used for the calculation of AEM diffusion and dimer formation energy barriers, respectively. The local minimum was found through the conjugate-gradient technique and employing DFT calculations performed with a 4 $\times 4 \times 1$ **k**-point grid for electronic sampling.

For molecular dynamics (MD) simulations, we used the Born-Oppenheimer scheme where the self-consistent ground state is recalculated at each MD time-step. A Verlet-type algorithm and Nosè thermostat were used for integration of Newton's equations of motion and (N, V, T) canonical ensemble sampling, respectively. Supercells used in the AIMD simulations contained 9 AEM and 54 C atoms for graphene, and 10 AEM and 40 C atoms for CNT; due to the intensive computational workload associated to these simulations we employed electronic Γ-point sampling only. The total duration of a typical AEM-carbon nanostructure molecular dynamics run was 15–20 ps, being 2×10^{-3} ps the time step used. Initial configurations in the AIMD simulations were taken from the atomic structural relaxations and temperature was varied from 300 up to 900 K at 300 K intervals.

Standard GGA-DFT is an affordable first-principles computational technique that has proved successful at reproducing accurately metallic, covalent and ioniclike bonds,[41,42] however, this scheme appears to be not so precise at describing weak noncovalent interactions such as dispersive van der Waals forces and hydrogen bonds.[43–50] Relevant to this work and to biological systems as well is the metal cation-π
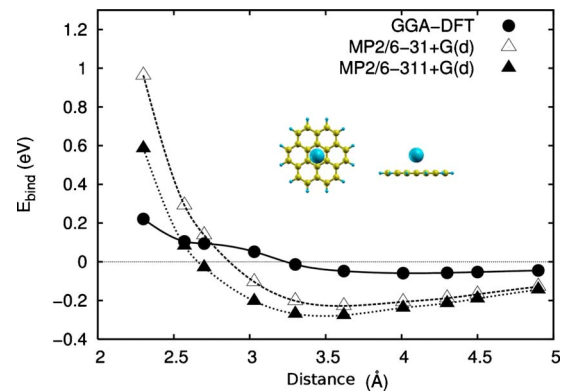

FIG. 1. (Color online) DFT-GGA and MP2 binding energy curves calculated for a system composed of a coronene molecule $C_{24}H_{12}$ and calcium atom. Different views of the Ca-coronene system are shown where H, C, and Ca atoms are represented with blue, yellow, and large blue spheres, respectively.

interaction,[51,52] a noncovalent electrostatic force that occurs between the face of an electron-rich π-system (e.g., benzene, graphene, etc.) and an adjacent cation (e.g., Li$^+$, Ca^{+2}, etc.). (It will be shown later that upon adsorption Ca atoms transfer a considerable amount of electronic charge to the nanostructures, so effectively they behave as cations). Cation-π energies are of the same order of magnitude as hydrogen bonds and they have already been studied with DFT and other more intricate and accurate computational approaches such as MP2 and coupled clusters [CCSD and CCSD(T)].[53,54]

For the particular case of Ca(cation)-nanostructure (π) interactions, we did not find any previous study contrasting the performance between GGA-DFT in the PBE flavour and high-level quantum chemistry methods, so we considered as interesting to carry out a calculation of this type. To this end, we studied the binding energy of a system composed of one coronene molecule, $C_{24}H_{12}$, and one calcium atom (see Fig. 1) using both GGA-DFT and MP2 approaches. MP2 calculations[55,56] were performed using 6-31+G(d) and 6-311+G(d) basis sets (that is, considering polarization and diffuse functions)[57,58] as implemented in the GAUSSIAN 03 package.[59] Basis set superposition errors were corrected using the counterpoise recipe.[60,61] We initially geometry optimized the coronene structure using GGA-DFT and then placed the Ca atom at a normal distance of 2.30 Å from the center of its plane (see Fig. 1); subsequently, the joint Ca-$C_{24}H_{12}$ system was left to relax using the GGA-DFT forces (neighboring images resulting from periodic boundary conditions were separated by a distance of 30 Å in order to avoid spurious interactions between them). From this geometry relaxation, we extracted a total of seven configurations and calculated the corresponding MP2 energies [no geometry optimization was performed at the MP2/6-31+G(d) or 6-311+G(d) level]. Three additional structures in which the calcium-coronene distance was increased beyond the GGA-DFT equilibrium value were also considered.

In Fig. 1, we show the GGA-DFT and MP2 binding energies calculated for these configurations. It is found that the equilibrium Ca-$C_{24}H_{12}$ distance and E_{bind} values obtained

with GGA-DFT are −0.060 eV and 3.84 Å while the MP2/6-311+G(d) method leads to −0.276 eV and 3.65 Å [MP2/6-31+G(d) values are −0.230 eV and 3.65 Å, respectively]. Assuming that MP2/6-311+G(d) results are the most accurate, one finds that GGA-DFT in the PBE flavour underestimates metal cation-π interaction energies significantly and overestimates the corresponding equilibrium distances. Comparison between MP2/6-311+G(d) and MP2/6-31+G(d) curves in Fig. 1, shows fair convergence of the energies with respect to the basis set, though it is likely that the use of improved basis sets (e.g., cc-ppVDZ, cc-pVTZ, etc.) would lead to further stabilization of the Ca-coronene system.

The conclusion emerging from this test is that weak Ca-π interactions are considerably underestimated using the GGA(PBE)-DFT method. Related computational studies carried out by Sun *et al.*[62] and Zhao *et al.*[63] on Ca-doped aromatic hydrocarbon systems, showed similar underestimation of the electronic correlations using the GGA(B3LYP)-DFT method. An interesting question that raised while carrying out the present benchmark test was, is the Ca-$C_{24}H_{12}$ system physically similar to Ca-decorated graphene?, or in other words, is it correct to extrapolate conclusions found in the Ca-$C_{24}H_{12}$ system to Ca-decorated nanostructures? Customarily, the study of the interactions of the coronene molecule, or even smaller organic systems such as benzene, with doping substances and/or other molecules using highly accurate computational methods such as MP2 or CCSD is performed in order to benchmark DFT.[44,45,64,65] In fact, the $C_{24}H_{12}$ molecule resembles closely to the structure of graphene and its reduced size allows for affordable high-level quantum chemistry calculations, thus generally conclusions obtained in medium-size organic molecule systems are assumed to be valid also in graphene. Strikingly, CDD analysis performed in both fully relaxed Ca-coronene and Ca-decorated graphene systems indicates that in the present case this assumption is not correct. Particularly, calculations reveal that in the Ca-$C_{24}H_{12}$ system the metal atom donates an electronic charge of $0.08e^-$ to the coronene molecule (weak interaction) while in Ca-decorated graphene it supplies about $0.9e^-$ (strong interaction). In fact, as it will be shown later, GGA-DFT binding energies obtained in Ca-coated graphene and the Ca-coronene system differ practically by one order of magnitude. These results appear to suggest important differences in the electronic structure of both systems and call for caution at claiming good or bad performance of DFT at describing binding properties of infinite systems based on benchmark results obtained in finite-size systems. We will comment again on this issue in Sec. III B.

III. RESULTS

A. Clusters versus bulk

As noted in Sec. I, the cohesive energy of bulk crystals E_{coh}^{bulk} in general is much smaller than that of finite clusters E_{coh}^{clust}. (By cohesive energy we mean minus the energy per particle required to break an entity into isolated atoms.) Consequently, when evaluating the stability of AEM-decorated nanostructures one cannot conclude with certainty that clustering of atoms will be favored over dispersion if the energy
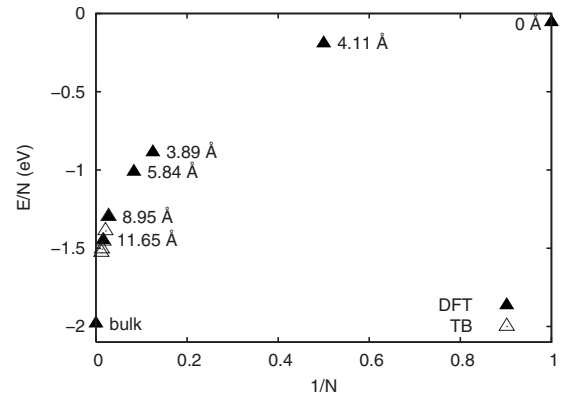

FIG. 2. Cohesive energy of Ca clusters as a function of the inverse of the number of atoms. Averaged cluster sizes are also indicated in the figure. DFT results correspond to present work and TB results are taken from Ref. 66 (see text for explanation).

difference $\Delta E = E_{bind} - E_{coh}^{bulk}$ is positive but "small," that is, of the same order of magnitude as $E_{coh}^{clust} - E_{coh}^{bulk}$ (contrarily, if $\Delta E \leq 0$ certainly one can conclude that coating is thermodynamically more favorable than clustering). Aimed at quantifying the order of magnitude of small, we geometry optimized a series of Ca clusters in vacuum ranging from few atoms up to 64, and compared the resulting cohesive energies with that of bulk solid Ca (face-centered cubic crystal structure).

Initial cluster configurations were generated by replicating the unit cell of the fcc crystal along the directions of its primitive vectors. For bulk fcc Ca, we calculated the corresponding zero-temperature equation of state considering only atomic perfect lattice configurations and found the equilibrium lattice parameter to be $a_0 = 5.50$ Å, which is in good agreement with the experimental value $a_0^{expt} = 5.58$ Å. According to our calculations, the cohesive energy of fcc Ca at equilibrium is $E_{coh}^{bulk} = -1.925$ eV/atom. (Similarly, we obtained $E_{coh}^{bulk} = -1.509$ eV/atom for hcp Mg at zero pressure.) In Fig. 2, we plot the results of our cluster geometry optimizations as function of the inverse of the number of atoms; as can be observed, the energy difference between large clusters of nanometer size and bulk fcc Ca is ~ 0.5 eV/atom. In fact, it is very likely that the atomic configurations and cohesive energies that we obtained upon geometry optimization correspond just to local (not global) energy minima since the initial configurations that we employed may be very different from true ground-state cluster structures. Because of these concerns, we compared our cluster-energy results with those obtained by Dong *et al.*,[66] who used an accurate tight-binding Hamiltonian to model the Ca-Ca interactions and an intricate combination of molecular dynamics-simulated annealing and genetic algorithms for the search of optimal structures. We found that the error associated to our $E_{coh}^{clust} - E_{coh}^{bulk}$ results is of order 0.01 eV/atom (see Fig. 2). For instance, we found a cohesive energy of $E_{coh}^{clust} = -1.300$ (−1.368) eV/atom for a cluster of 36 (48) atoms while Dong *et al.* obtained −1.298 (−1.389) eV/atom. In the light of these results, it can be concluded that energy differences in the range of $0 \leq E_{bind} - E_{coh}^{bulk} \leq 0.5$ eV/atom are not large

TABLE I. Binding energy per atom of AEM-coated graphene at different AEM coverages. $d_{\text{Ca-Gr}}$ represents the normal distance between the graphene sheet and AEM monolayer. ΔQ is the averaged electronic charge that one AEM atom donates to the carbon surface. Energies are expressed in units of electron volt, distance in angstrom, and charge in e^-.

Concentration (%)	Calcium				Magnesium			
	E_{bind}	$E_{bind}-E_{coh}^{bulk}$	$d_{\text{Ca-Gr}}$	ΔQ	E_{bind}	$E_{bind}-E_{coh}^{bulk}$	$d_{\text{Mg-Gr}}$	ΔQ
3.12	−0.443	1.482	2.26	0.86	−0.027	1.482	3.89	0.03
6.25	−0.887	1.038	2.31	0.79	−0.099	1.410	3.63	0.08
9.38	−1.074	0.851	2.36	0.63	−0.351	1.158	3.10	0.20
12.50	−1.197	0.728	2.28	0.71	−0.362	1.147	3.60	0.10
16.67	−1.594	0.331	2.34	0.62	−0.519	0.990	3.68	0.08
25.00	−0.056	1.869	2.22	0.53	−0.054	1.455	3.20	0.17
50.00	2.093	4.018	2.20	0.39	0.292	1.801	4.21	0.01

enough to confidently state that uniform AEM coatings are unstable with respect to formation of aggregates. In fact, some of the ΔE values that we will report in the next sections, and some reported by other authors as well, lie within this range of uncertainty thus one has to be very cautious at making stability statements for Ca-decorated nanostructures.

One likely strategy for prediction of AEM uniform coating or aggregation tendencies may consist in performing systematic geometry optimization of clusters of increasingly large sizes on top of the carbon nanosurfaces. This strategy, however, poses two important technical problems. First, geometry optimizations performed with *ab initio* forces turn out to be computationally very demanding so in practice only clusters of small or medium sizes could be studied (it must be kept in mind that C atoms in the nanostructures should be also considered in the structural relaxations). Second, and most importantly, is that the free-energy landscapes of joint AEM-nanostructure systems can be extremely intricate so that reaching global energy minimum configurations might prove elusive despite the existence of very effective structure search algorithms.

In view of the intricacies posed by this method, we opted for a more straightforward approach. This consisted in obtaining first the most stable uniformly AEM-coated nanostructures by exploring a range of coverages and possible atomic arrangements, and then performing long duration AIMD simulations with them. In the dynamical simulations, ambient and also higher temperatures were considered ($300\ \text{K}\le T\le 900\ \text{K}$). Finally, transition energy barriers corresponding to atomic diffusion and AEM-dimer formation processes in the carbon surfaces were calculated in order to help understanding the AIMD outcomes and assess possible kinematic effects.

B. AEM-decorated graphene

In our simulations, we used a $4\times 4\times 1$ graphene unit cell containing 32 C atoms that was filled progressively with AEM atoms (from 1 up to 16). AEM concentration and/or coverage terms here refer to the ratio between the number of Ca (Mg) and C atoms (for instance, a concentration of 3.12%

corresponds to 1 Ca atom per one $4\times 4\times 1$ graphene unit cell). Only one side of the graphene sheet was considered for AEM coating. We started exploring the case of one isolated Ca and Mg atom in customary *hollow* (center of C hexagons), *bridge* (on top of C-C bonds) and *on-top* (on top of C atoms) graphene adsorption sites. In the Ca case, *hollow* adsorption site was energetically more favorable than *bridge* and *on-top* conformations by about 0.10 eV. Mg atoms also showed a preference for *hollow* adsorption sites but in this case only by a small energy difference of 0.001 eV. In order to infer the preferred adsorption sites at large metal concentrations, we also analyzed the case of two Ca atoms adsorbed both in *hollow*, *bridge* and *on-top* positions and separated by a distance of 4.3 Å (e.g., three times the C-C bond length). In this case we also found that *hollow* adsorption sites was energetically the most favorable geometry by an energy difference of 0.08 and 0.09 eV/atom with respect to *bridge* and *on-top* conformations. In view of these results, the configurational space of AEM atoms at given concentration was sampled thoroughly considering only *hollow* adsorption sites in the initial nonoptimized geometries (though atoms were left to move freely to other adsorption positions along the atomic relaxations).

In Table I, we report results for the energetically most favorable Ca and Mg-decorated structures that we obtained in our simulations (see also Fig. 3). These results demonstrate that AEM-coated graphene becomes progressively
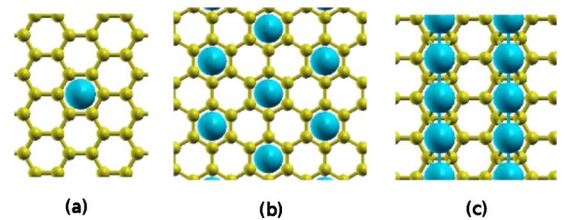

FIG. 3. (Color online) Energetically most favorable Ca-decorated graphene structures obtained at 3.12% (a), 16.67% (b), and 25.00% (c) calcium concentration. Configuration (b) corresponds to the equilibrium structure found, namely, a commensurate $(\sqrt{3}\times\sqrt{3})$ R30° CaC$_6$ monolayer with lattice parameter $a=\sqrt{3}a_G$ ($a_G=2.49$ Å).

more stable as AEM coverage is increased up to a equilibrium concentration of 16.67% (this concentration is equal to 1 Ca atom per 6 C atoms). In both Ca and Mg cases, we found that the equilibrium monolayer structure corresponds to a commensurate $(\sqrt{3} \times \sqrt{3})$ R30° lattice [see Fig. 3(b)] with parameter $a = \sqrt{3} \, a_G$ ($a_G = 2.49$ Å). The area density of particles in this equilibrium structure is 0.061 atom/Å^2. It is worth noticing that analogous monolayer patterns have been observed in bulk calcium graphite CaC$_6$ (Refs. 67 and 68) and ^{4}He films deposited on top of graphite and graphene.[69,70] At coverages higher than 16.67%, the binding energy of AEM coatings decreases noticeably due to repulsive AEM-AEM Coulombic interactions that appear as a consequence of the electronic charge donations to the carbon surface (see ΔQ columns in Table I).

In spite of the explained similarities, Ca- and Mg-decorated graphene present quite different binding features. In fact, Ca atoms adhere to the carbon surface more strongly than Mg atoms do (see columns E_{bind}, $d_{Ca\text{-}Gr}$, and $d_{Mg\text{-}Gr}$ in Table I) and this effect is correlated with large (Ca) or negligible (Mg) electronic charge transfers to graphene (see columns ΔQ in Table I). As we will shown later in this section, the origins of large electronic charge transfers, and then strong dopant binding, in Ca-decorated graphene can be explained in terms of the arguments already provided by Yoon *et al.*[23] for fullerene systems, namely, electronic s(metal) $- \pi$ band (graphene) interactions and consequent charge back donation to unoccupied d(metal)-states. Since in Mg-decorated graphene electronic d-states in the conduction energy band are lacking, charge back-donation processes do not occur and consequently the dopant binding is not reinforced as in the Ca case.

Regarding the stability of AEM-decorated graphene systems, we enclose in Table I the value of the corresponding $\Delta E = E_{bind} - E_{coh}^{bulk}$ energy differences. For Ca-coated graphene, it is seen that only the ΔE value corresponding to the equilibrium CaC$_6$ monolayer configuration lies within the range of uncertainty $0 \leq \Delta E \leq 0.5$ eV/atom that we set in Sec. III A. Based on our aforementioned arguments, we cannot ensure then stability or instability of this structure against clustering. In contrast, uniformly Mg-decorated graphene appear to exhibit a clear tendency for Mg aggregation since all the calculated ΔE values are noticeably larger than 0.5 eV/atom. In order to assess the stability of the equilibrium CaC$_6$ and MgC$_6$ monolayer structures found, we carried out a series AIMD simulations with them (technical details of these simulations are explained in Sec. II).

In Fig. 4, we show the results of these AIMD simulations in which the diffusion of the center of mass (CM) of AEM $(\sqrt{3} \times \sqrt{3})$ R30° monolayers are plotted as function of time. In the same figure, we also represent the trajectory of the CM of AEM monolayers projected on the graphene plane (arbitrarily defined as x-y). These plots monitor the atomic displacements within the monolayers and we refer them to the center of mass of graphene or initial configurations in order to facilitate their interpretation. In Ca-coated graphene, essentially flat CM diffusion profiles exhibiting some small fluctuations are obtained at temperatures as elevated as 900 K and long simulation times. These patterns demonstrate that commensurate $(\sqrt{3} \times \sqrt{3})$ R30° CaC$_6$ monolayer is certainly
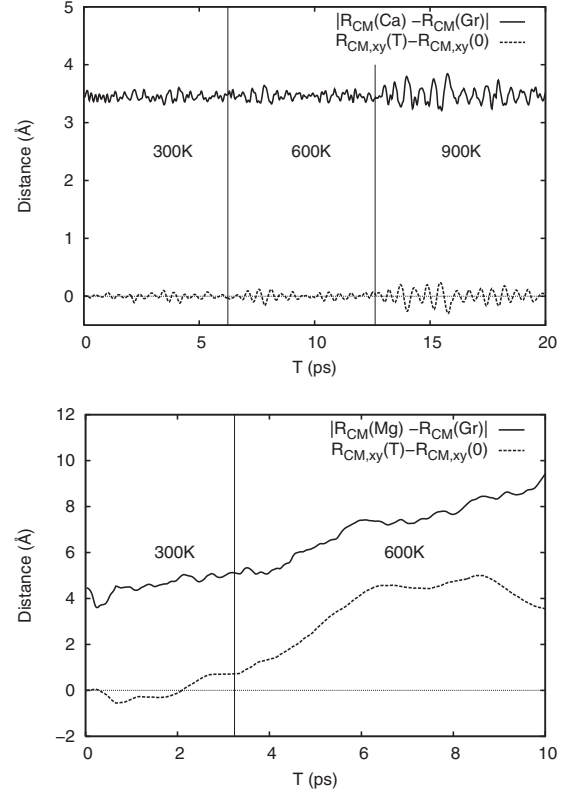

FIG. 4. Diffusion of the center of mass of AEM $(\sqrt{3} \times \sqrt{3})$ R30° monolayers (Top: Ca, Bottom: Mg) referred to the center of mass of graphene (solid line). AEM center of mass trajectories projected on the graphene x-y plane are also shown (dashed line). These results were obtained over long (N, V, T) *ab initio* molecular simulations in which temperature was varied from 300 to 900 K.

stable at low and room temperatures despite its corresponding ΔE value of 0.331 eV/atom. In contrast, the center of mass of the Mg coating is observed to get increasingly distant from the graphene plane even at low temperatures. This result shows clear instability of the commensurate $(\sqrt{3} \times \sqrt{3})$ R30° MgC$_6$ monolayer since Mg atoms migrate out of the carbon surface. Visual recreation of the atomic configurations generated along the AIMD runs corroborates these conclusions.

As noted in Sec. I, the stability of a material such as AEM-decorated graphene also depends on the kinetic energy barriers governing the mobility of AEM atoms. For that reason, we analyzed two simple transition processes related to AEM aggregation, namely, atomic diffusion and AEM-dimer formation. For the atomic diffusion process, we considered the center of two contiguous carbon hexagons as the initial and final positions of one migrant atom (see Fig. 5). For AEM-dimer formation process, we considered two AEM atoms adsorbed on two neighboring *hollow* sites as the initial configuration, and one atom positioned on top of another, adhered to graphene, as the final configuration (see Fig. 6). This is a simple process that is far from reproducing clustering of a large number of atoms, however, it provides an estimation of the energy barriers involved in atomic rearrangements that may lead to the formation of three-dimensional structures.
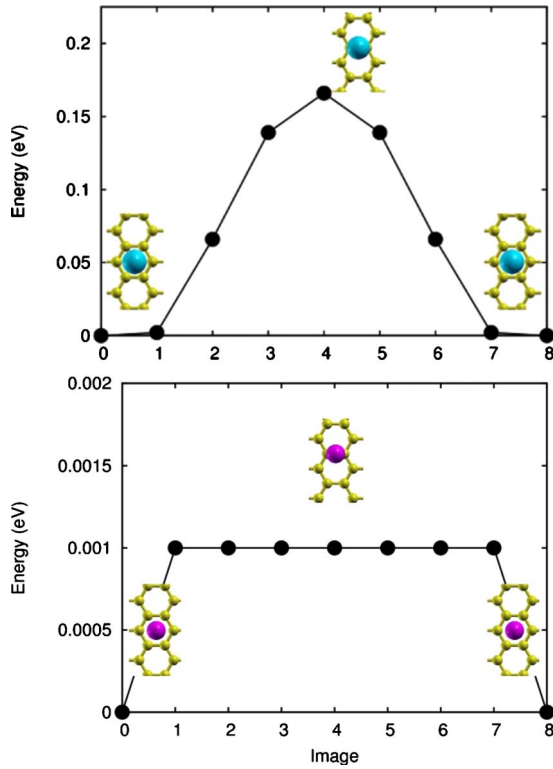
FIG. 5. (Color online) Minimum energy transition path for *hollow→hollow* diffusion of one isolated Ca (Top) and Mg (Bottom) atom on graphene. Initial (image 0), saddle and final (image 4) configurations are shown.
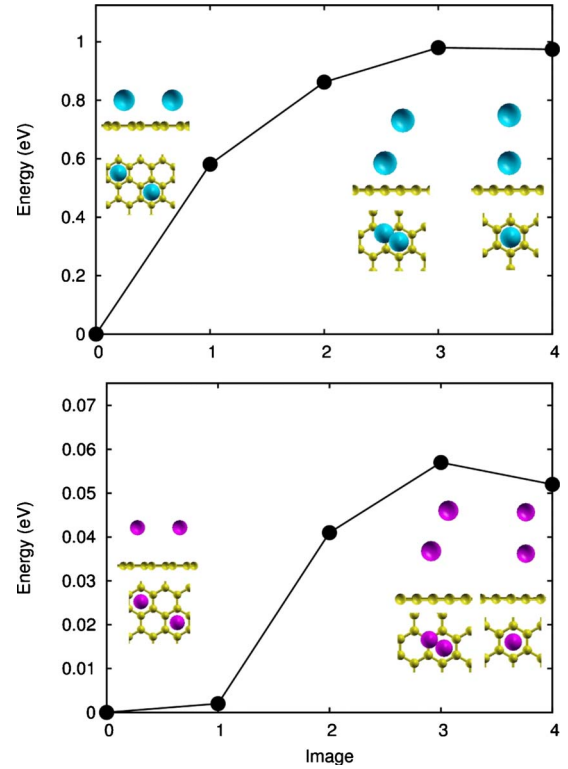

FIG. 6. (Color online) Minimum energy transition path for Ca- and Mg-dimer formation on graphene (Top and Bottom, respectively). Initial (image 0), saddle and final (image 4) configurations are shown.

We used the NEB method to determine the minimum energy transition paths corresponding to these processes (see Figs. 5 and 6). For atomic diffusion, we found an energy barrier of 0.001 eV and 0.168 eV for Mg and Ca, respectively. This result indicates that Mg atoms are much more mobile than Ca atoms in the graphene surface, as already it was shown in the AIMD simulations. The cause of the large difference between Mg and Ca atomic mobilities is related to the amount and variation in AEM electronic charge transferred to graphene along the transition paths. In particular, Ca atoms in *bridge* adsorption sites (saddle energy point) donate ~10% less electronic charge than in *hollow* adsorption positions. In Mg-doped systems, however, atomic charge differences between *bridge* and *hollow* configurations are practically zero. Regarding the formation of AEM-dimers, we obtained an energy barrier of 0.058 eV for Mg and of 0.980 eV for Ca. Again the origins of the large difference between Ca and Mg energy barriers can be understood in terms of the magnitude and variation in AEM electronic charge transfers, which in the case of Mg atoms are both always very small. As can be observed, the energy barrier calculated for Ca-dimer formation is quite large and appreciably higher than the one obtained for atomic diffusion. This outcome shows that, despite Ca atoms being quite mobile on the graphene surface, mild thermodynamic forces driving them to cluster may be kinematically hindered. Consequently, two-dimensional CaC_n structures exhibiting $\Delta E = E_{bind} - E_{coh}^{bulk}$ values larger than but close to 0.5 eV/atom (e.g., Ca coatings obtained at 12.5% and 9.4% concentra-

tions, see Table I) could be also observed in practice.

In Sec. II, we presented the results of a test in which we compared the performance of DFT and MP2 methods at describing weak cation-π interactions in a Ca-$C_{24}H_{12}$ system. The main conclusion of that test is that DFT appears to underestimate cation-π energies significantly. Consequently, DFT stability predictions in Ca/C-based materials where the cross metal-framework interactions are very weak can be regarded only as qualitatively correct. Interestingly, we also found that the Ca-coronene and Ca-doped graphene systems cannot be considered as physically equivalent based on binding energy and charge density distribution analysis. In order to rationalize the origins of these differences we computed the electronic density of states (DOS) of both Ca-coronene and Ca-doped graphene systems accurately, and in Fig. 7 we plot the resulting partial *s*, *p*, and *d* components. In fact, the calculated DOS profiles turn out to be appreciably different, namely (i) strong hybridization between *p* (graphene) and *s-d* (Ca) electronic orbitals near the Fermi energy level E_F is found in Ca-doped graphene but not in the Ca-coronene system, and (ii) the cloud of *d* electronic states spreads over a wider range of energies in Ca-graphene. Strong hybridization between *p* carbon and *s-d* metal orbitals, therefore, emerges as the likely cause for the disparities found between the coronene and graphene-based systems, and can also explain the origin of the weak metal binding observed in Mg-decorated graphene where electronic *d*-states in the conduction energy band are missing. It is worth noting that our Ca-decorated graphene DOS results are consistent with those found previ-
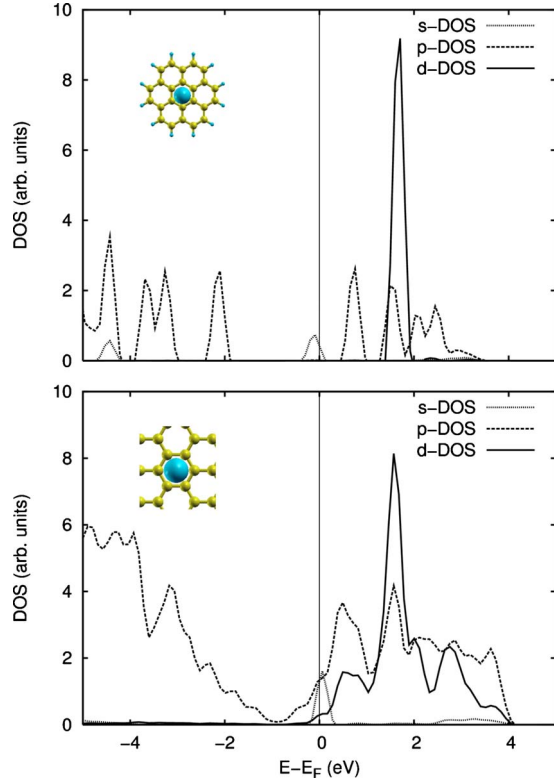
FIG. 7. (Color online) Partial density of electronic states obtained in geometry optimized Ca- coronene (Top) and Ca-doped graphene (Bottom) systems.

ously by Calandra *et al.*[71] in metal-doped graphene and also by Yoon *et al.* in Ca-decorated fullerenes.[23] The last conclusion presented in this section, namely, nonelectronic structure equivalence between Ca-doped graphene and Ca-coronene systems, may serve as a warning that results obtained in small Ca-doped systems (as for instance, results

of computational benchmark tests) in principle cannot be generalized straightforwardly to infinite Ca-decorated systems because the nature of the atomic interactions involved in both systems can be completely different. Interestingly, Sun *et al.*[62] have shown recently that Ca binding to one benzene molecule can be enhanced substantially by increasing the number of Ca dopants. Such an enhancement of the metal-benzene interactions is explained in terms of a $sp^2 \rightarrow sp^3$ orbital hybridization electronic transition which is accompanied of a significant structural distortion of the benzene molecule. In view of Sun's results and ours already presented, one could suggest a likely route for realization of fully meaningful yet still affordable computational benchmark tests for infinite metal-doped carbon systems; this will consist in performing the required high-level/low-level energy calculations in small aromatic hydrocarbon systems (e.g., benzene, antracene, coronene, etc.) where the number of metal dopants would be increased in order to reproduce as closely as possible the electronic structure features of the infinite system of interest.

C. AEM-decorated CNTs

In Table II, we report energy results for atomic Ca and Mg binding on a series of CNTs obtained as function of concentration. Aimed at analyzing the effect of CNT radius and chirality, we considered four different CNT structures, namely (10, 0), (6, 0), (6, 6), and (4, 4). Since the radius of the (10, 0) and (6, 6) nanotubes, on one hand, and of the (6, 0) and (4, 4), on the other, are very similar, CNT radius and chirality effects can be studied separately. Results shown in Table II have been obtained by performing geometry optimization of the following structures; the first row in any of the columns corresponds to one isolated atom adsorbed on the center of one C hexagon (this configuration turned out to be the minimum energy configuration in all the studied cases);

TABLE II. $\Delta E = E_{bind} - E_{coh}^{bulk}$ energy differences of Ca-decorated CNTs as function of Ca concentration (equal to the ratio between the number of Ca and C atoms). d_{Ca-Ca} and ΔQ represent averaged interatomic calcium distance (over first- and second-nearest neighbors) and electronic charge per atom donated to the carbon nanotube, respectively. Numbers within parentheses correspond to Mg-decorated CNTs (sign - indicates formation of clusters upon geometry optimization). Energies are in units of electron volt, distance in angstrom, and electronic charge in e^-.

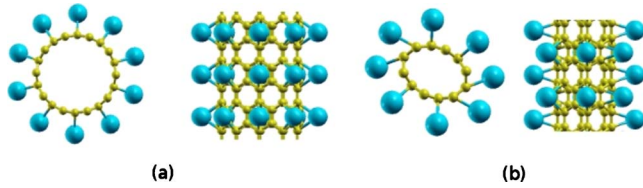| Concentration (%)	(10,0) R=3.96 Å			(6,0) R=2.42 Å			(6,6) R=4.12 Å			(4,4) R=2.77 Å		
	ΔE	d_{Ca-Ca}	ΔQ	ΔE	d_{Ca-Ca}	ΔQ	ΔE	d_{Ca-Ca}	ΔQ	ΔE	d_{Ca-Ca}	ΔQ
1	1.154 (1.486)	4.26	1.37				1.324 (1.477)	7.40	0.99			
2	0.782 (1.414)	3.86	0.83							1.147 (1.469)	9.76	1.19
3							0.772 (1.229)	5.45	0.68	0.782 (1.384)	8.14	0.79
4				0.169 (1.329)	4.28	0.89						
8	0.593 (1.218)	3.93	0.75	0.130 (0.926)	3.93	0.78						
12	0.541 (1.137)	3.98	0.72									
18	0.516 (0.906)	4.00	0.63									
25	0.464 (-)	4.03	0.72				0.798 (-)	5.47	0.66	0.727 (-)	4.41	0.65
30	0.379 (-)	4.00	0.57									
33				0.115 (-)	4.08	0.75						
38				0.092 (-)	3.98	0.67						

FIG. 8. (Color online) Geometry optimized Ca-decorated CNT structures obtained at moderately large doping coverage. Left (a): views of (10, 0) nanotube decorated at 30% Ca concentration. Right (b): views of (6, 0) nanotube doped at 38% Ca concentration.

the second line corresponds to two atoms adsorbed on the center of two contiguous hexagons; the rest of rows correspond to uniform AEM coatings where Ca and Mg atoms do not necessarily accommodate in the center of C six-rings.

According to our results, some general Ca-CNT binding trends can be identified: (i) $(n,0)$ zigzag binding energies are smaller than those calculated in (n,n) armchair CNTs of similar radius, (ii) the smaller the radius of zigzag nanotubes the more attractive the Ca-CNT interactions turn out to be, (iii) zigzag Ca-decorated CNTs are further stabilized at moderately large doping concentrations, and (iv) (n,n) armchair CNTs do not systematically follow trend (iii) observed in $(n,0)$ zigzag nanotubes. Results (i) and (ii) are in agreement with conclusions found by Yang *et al.*[24] in Ca-decorated (5, 0), (4, 0), and (3, 3) nanotubes. The authors of that work argue that the observed energy trends can be understood in terms of Coulombic Ca-Ca and C-C repulsive interactions that emerge as result of significant electronic charge rearrangements within the systems; those repulsive forces turn out to be minimized more effectively in zigzag nanostructures than in armchair CNTs due to their topology, and as the CNT radius is reduced Ca-Ca distances develop larger so that repulsive forces are softened. Our electronic density of states and charge density distribution analysis performed in Ca-decorated (6, 0) and (4, 4) CNTs do corroborate Yang's hypothesis. Nevertheless, the authors of Ref. 24 claim that Ca-decorated CNT become unstable with increasing Ca coverage, a conclusion that apparently is in conflict with our results. In fact, one may reasonably expect that large Ca doping concentrations will destabilize CNTs due to intense Ca-Ca interatomic repulsions, similarly to what we found in Ca-decorated graphene (see Table I in Sec. III B). However, columns ΔQ in Table II show that as Ca coverage is increased the amount of electronic charge transferred to CNTs decreases, so that there must exist a maximum Ca coverage for each CNT below which attractive Ca-CNT interactions still outweigh the repulsive Coulombic energy. In (10, 0) and (6, 0) CNTs, we set this limit to 30% and 38% Ca concentrations, respectively, (see Fig. 8) though even larger values could be attained. It is worth noting that in most of the studied cases the Ca-Ca distances averaged over first- and second-nearest neighbors turn out to be larger than the minimum interatomic distance found in bulk fcc Ca at equilibrium (d_{Ca-Ca}^{bulk}=3.89 Å).

In Fig. 9, we plot the dependence of atomic Ca binding energy on the inverse of zigzag CNT radius as obtained at low doping concentrations (e.g., 1–5 %). We further studied the CNT cases (8, 0) and (15, 0), not shown in Table II, in
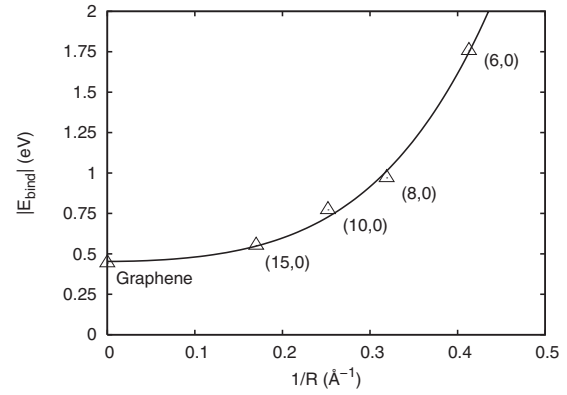

FIG. 9. Calcium binding energy as a function of the inverse of zigzag CNT radius obtained at low-doping concentrations (1–5 %). Graphene is considered as a limiting case of CNT with infinite radius.

order to provide an accurate and reliable numerical fit to our results. Considering graphene as a limiting case of CNT with infinite radius, it was found that the polynomial expression $E_{bind}=a+b(1/R)^2+c(1/R)^4$ with parameter values a =0.453 eV, b=2.40 eV Å^2 and c=30.38 eV Å^4 reproduced our calculated E_{bind} values within less than 0.05 eV/atom. As we have already mentioned, Ca binding clearly increases with decreasing CNT radius, or equivalently, with increasing CNT curvature. Apart from the fact that increasing CNT curvature leads to smaller Ca-Ca repulsive interaction because the distance between cation centers then develops larger, some electronic structure effects may also have a role in this. We refer here to the distorsion-induced $sp^2 \rightarrow sp^3$ electronic hybridization phase transition found by Sun *et al.* in a Ca-doped benzene molecule system,[62] already commented in Sec. III B. In particular, hybridized sp^2 orbitals localized in neighboring carbon atom positions appear to pose less resistance to electronic Ca penetration as the angle sustained by their out-of-plane symmetry axis increases by effect of surface curvature. It is worth stressing that results shown in Fig. 9 were obtained at low-doping concentrations so that the already explained binding energy trends probably cannot be generalized to large Ca densities.

Conclusions regarding Mg-decorated CNTs are analogous to those found in AEM-decorated graphene, namely, very weak Mg-CNT binding due to lack of electronic π (CNT)-d (metal) orbitals hybridization. At large coverages, we already observed destabilization of the uniform Mg coatings upon geometry optimization. This result shows that these structures are neither total nor local minimum energy configurations (in Table II, we indicate this effect as -) and that there exist intense thermodynamic forces driving them to cluster.

Next, we comment on the stability of Ca-decorated CNTs. The energy differences reported in Table II show that Ca-decorated zigzag CNTs are likely to be stable at moderately large coverages (e.g., 30–40 %) since the corresponding $E_{bind}-E_{coh}^{bulk}$ values amount to less than 0.5 eV/atom. In contrast, armchair nanotubes exhibit a clear tendency for Ca aggregation (as recently was pointed out by Lee *et al.* in Ref. 26). We chose the 25% Ca-decorated (10, 0) CNT to perform molecular dynamics simulations because this structure ap-
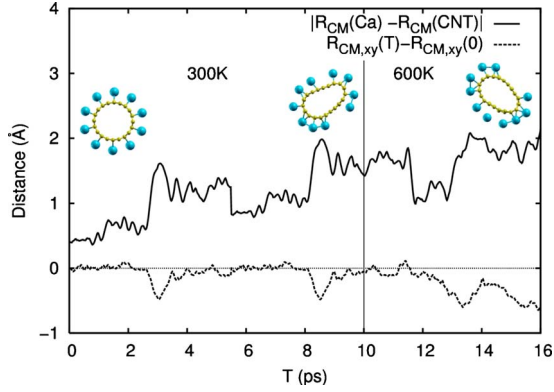
FIG. 10. (Color online) Diffusion of the center of mass (CM) of the (10, 0) CNT 25% Ca coating referred to the center of mass of the nanotube (solid line). The center of mass trajectory of the Ca coating projected on the x-y plane is also represented (dashed line). Results were obtained over a long (N, V, T) *ab initio* molecular simulation in which temperature was varied from 300 to 600 K; some representative configurations generated along these simulations are shown in the figure.

pears to be on the verge of likely stability and then it can be considered as a limiting case. In Fig. 10, we plot the diffusion of the CM of the Ca coating referred to that of the (10, 0) CNT at different temperatures. The calculated CM trajectories show that despite Ca atoms diffuse on the CNT surface, an effect that probably is enhanced by temperature-induced CNT deformations (see Fig. 10), there is not nucleation of three-or quasi two-dimensional structures (that is, Ca atoms always remain attached to the carbon surface). Therefore, according to our definition of clustering and to trend (ii) cited above, densely Ca-decorated $(n, 0)$ zigzag CNTs with $n \leq 10$ appear to be stable at room temperature. We note that the CM profiles enclosed in Fig. 10 are not as flat as those calculated in Ca-decorated graphene (see Fig. 4), however, this effect is just a consequence of larger spatial fluctuation of the CNT center of mass itself. Our conclusion concerning the stability of zigzag CNTs is in accordance with results reported by Yang *et al.* in Ref. 24 though we demonstrate that the limit of stability of $(n, 0)$ nanotubes can be expanded to CNT radii of at least ~4 Å.

Furthermore, we calculated the energy barriers corresponding to Ca diffusion and dimer formation on the surface of zigzag and armchair nanotubes. For atomic diffusion, we obtained small energy barriers of ~0.1 eV in all the studied cases; saddle point configurations turned out to coincide with *bridge* adsorption sites. This result appears to be consistent with large Ca mobility observed in the dynamical simulations. In Fig. 11, we present NEB results obtained for Ca-dimer formation in the outer surface of a (6, 0) CNT for which an energy barrier of 0.855 eV was calculated. Similarly, we obtained transition energy barriers of 0.690 eV, 0.904 eV, and 0.800 eV for (10, 0), (6, 6), and (4, 4) CNTs, respectively. It was found that saddle energy point configurations always coincided with final Ca-dimer structures. In view of the large Ca-dimer formation energy barriers calculated, observation of Ca-decorated armchair CNTs cannot be completely ruled out since these structures could be kinematically stabilized in practice.
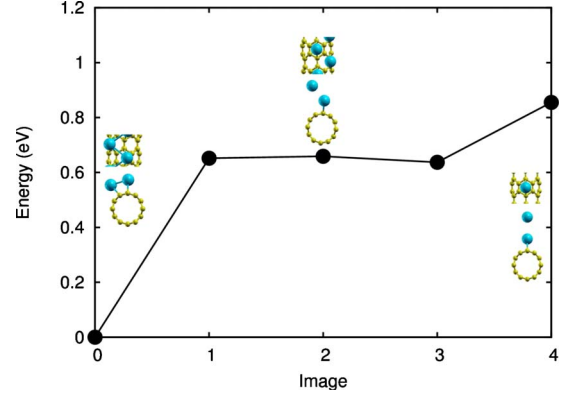

FIG. 11. (Color online) Minimum energy transition path for Ca-dimer formation on the outer surface of a (6, 0) CNT. Initial (image 0), intermediate and final (also saddle, image 4) configurations are shown.

We note that a useful side benefit from our NEB simulations is that the energy barriers calculated could be employed as inputs in multi-scale kinetic Monte Carlo simulations involving a large number of Ca atoms and carbon-based nanostructures. This type of calculation is particularly well suited for modeling of catalytic processes in nanosurfaces and could also shed more light on the stability issues concerning Ca-decorated (n, n) CNTs.

IV. GENERAL DISCUSSION AND CONCLUSIONS

We analyzed the stability, structure, and binding energy properties of uniformly Ca-decorated graphene and nanotubes using density-functional theory. For graphene, we predicted the existence of an equilibrium $(\sqrt{3} \times \sqrt{3})$ R30° commensurate CaC_6 monolayer that is proved to be stable against clustering in *ab initio* molecular dynamics simulations performed at 300 K $\leq T \leq$ 900 K. Regarding CNTs, we found that the equilibrium Ca-coated $(n \leq 10, 0)$ nanostructures correspond to moderately large Ca coverages (e.g., ~30–40 %) and that these systems remain stable against clustering at room temperature. In contrast, armchair (n, n) nanotubes present a certain tendency for Ca aggregation independently of CNT radius and Ca concentration. Nevertheless, we found that Ca aggregation processes in carbon nanosurfaces may be effectively hindered due to the existence of significant kinetic effects.

Interestingly, we performed a computational test in which DFT was benchmarked with respect to the MP2 method at describing metal cation-π interactions in a system composed of a Ca atom and coronene molecule. It was found that DFT does underestimate the weak Ca dopant-$C_{24}H_{12}$ molecule binding appreciably, thus one is likely to predict further stability of Ca-decorated aromatic hydrocarbon systems using quantum computational approaches that go beyond DFT and treat the electronic correlations more accurately. We also concluded that from an electronic structure point of view the Ca-coronene and Ca-doped graphene systems cannot be regarded as physically equivalent. This finding may serve as a warning that results obtained in finite Ca-doped systems can-

not be generalized straightforwardly to infinite Ca-decorated nanostructures since the nature of the atomic interactions in both systems can differ greatly. Nevertheless, we also showed that calcium atoms bind very strongly to carbon nanostructures as a consequence of large electronic charge rearrangements that result from intense p (carbon) and $s-d$ (metal) orbital interactions. In the case of intense binding, the DFT method is expected to perform correctly both at the qualitative and quantitative levels so that the present study and previous related ones based also on the DFT approach can be considered as valid.

Recently, a number of theoretical works dealing with the hydrogen storage properties of Ca-decorated carbon nanostructures have been published.[23–28,32] In some of those works, the authors propose ways of further enhancing the stability of Ca adsorbates in carbon nanosurfaces.[26,27,32] Nevertheless, conclusions presented in this work, and reported by other researchers as well,[23–25] show that coating instability against clustering is not a crucial issue in Ca-decorated nanostructures. In fact, a drawback that appears to be more dramatic and needs to be addressed is likely dopant segregation from these nanomaterials due to large reactivity between the Ca atoms and gas molecules. For instance, Wood *et al.*[72] have shown recently that bulk calcium graphite, a promising gas storage nanomaterial,[73] becomes thermodynamically unstable with respect to decomposition into graphite and calcium hydride when loaded with H_2 gas, a conclusion that is consistent with experimental observations.[74] Certainly, by enhancing the stability of Ca adsorbates in carbon nanostructures the reactivity of Ca atoms with gas molecules can be somewhat depleted, however, dopant segregation occurrence needs to be addressed specifically in order to motivate experiments on feasible synthesis of novel nanomaterials.

ACKNOWLEDGMENTS

*c.silva@ucl.ac.uk

[1] S. Iijima, Nature (London) **354**, 56 (1991).

[2] M. S. Dresselhaus, G. Dresselhaus, and P. C. Eklund, *Science of Fullerenes and Carbon Nanotubes* (Academic Press, New York, 1996).

[3] M. L. Cohen, Science **261**, 307 (1993).

[4] K. S. Novoselov, A. K. Geim, S. V. Morozov, D. Jiang, M. I. Katsnelson, I. V. Grigorieva, S. V. Dubonos, and A. A. Firsov, Nature (London) **438**, 197 (2005).

[5] J. O. Sofo, A. S. Chaudhari, and G. D. Barber, Phys. Rev. B **75**, 153401 (2007).

[6] D. C. Elias, R. R. Nair, T. M. G. Mohiuddin, S. V. Morozov, P. Blake, M. P. Halsall, A. C. Ferrari, D. W. Boukhvalov, M. I. Katsnelson, A. K. Geim, and K. S. Novoselov, Science **323**, 610 (2009).

[7] J. Kong, N. R. Franklin, C. Zhou, M. G. Chapline, S. Peng, K. Cho, and H. Dai, Science **287**, 622 (2000).

[8] S. Peng and K. Cho, Nano Lett. **3**, 513 (2003).

[9] R. H. Baughman, C. Cui, A. A. Zakhidov, Z. Iqbal, J. N. Barisci, G. M. Spinks, G. G. Wallace, A. Mazzoldi, D. De Rossi, A. G. Rinzler, O. Jaschinski, S. Roth, and M. Kertesz, Science **284**, 1340 (1999).

[10] S. Tans, A. Verschueren, and C. Dekker, Nature (London) **393**, 49 (1998).

[11] A. C. Dillon, K. M. Jones, T. A. Bekkedahl, C. H. Kiang, D. S. Bethune, and M. J. Heben, Nature (London) **386**, 377 (1997).

[12] R. Singh, D. Pantarotto, D. McCarthy, O. Chaloin, J. Hoebeke, C. D. Partidos, and K. Kostarelos, J. Am. Chem. Soc. **127**, 4388 (2005).

[13] S. Meng, P. Maragakis, C. Papaloukas, and E. Kaxiras, Nano Lett. **7**, 45 (2007).

[14] X. Chen, A. Kis, A. Zettl, and C. R. Bertozzi, Proc. Natl. Acad. Sci. U.S.A. **104**, 8218 (2007).

[15] W. Yang, P. Thordarson, J. J. Gooding, S. P. Ringer, and F. Braet, Nanotechnology **18**, 412001 (2007).

[16] S. A. Shevlin and Z. X. Guo, J. Phys. Chem. C **112**, 17456 (2008).

[17] S. A. Shevlin and Z. X. Guo, Chem. Soc. Rev. **38**, 211 (2009).

[18] T. Yildirim and S. Ciraci, Phys. Rev. Lett. **94**, 175501 (2005).

[19] Y. F. Zhao, Y.-H. Kim, A. C. Dillon, M. J. Heben, and S. B. Zhang, Phys. Rev. Lett. **94**, 155504 (2005).

[20] Y. Zhang, N. W. Franklin, R. J. Chen, and H. Dai, Chem. Phys. Lett. **331**, 35 (2000).

[21] Q. Sun, Q. Wang, P. Jena, and Y. Kawazoe, J. Am. Chem. Soc. **127**, 14582 (2005).

[22] S. Li and P. Jena, Phys. Rev. Lett. **97**, 209601 (2006).

[23] M. Yoon, S. Yang, C. Hicke, E. Wang, D. Geohegan, and Z. Zhang, Phys. Rev. Lett. **100**, 206806 (2008).

[24] X. Yang, R. Q. Zhang, and J. Ni, Phys. Rev. B **79**, 075431 (2009).

[25] C. Ataca, E. Aktürk, and S. Ciraci, Phys. Rev. B **79**, 041406(R) (2009).

[26] H. Lee, J. Ihm, M. L. Cohen, and S. G. Louie, Phys. Rev. B **80**, 115412 (2009).

[27] H. Lee, J. Ihm, M. L. Cohen, and S. G. Louie, Nano Lett. **10**, 793 (2010).

[28] Y.-H. Kim, Y. Y. Sun, and S. B. Zhang, Phys. Rev. B **79**, 115424 (2009).

[29] H. S. Kang, J. Am. Chem. Soc. **127**, 9839 (2005).

[30] C. Cazorla, Thin Solid Films **518**, 6951 (2010).

[31] U. Zimmermann, N. Malinowski, U. Näher, S. Frank, and T. P. Martin, Phys. Rev. Lett. **72**, 3542 (1994).

[32] G. Kim, S.-H. Jhi, S. Lim, and N. Park, Appl. Phys. Lett. **94**, 173102 (2009).

[33] P. E. Blöchl, Phys. Rev. B **50**, 17953 (1994).

[34] G. Kresse and D. Joubert, Phys. Rev. B **59**, 1758 (1999).

[35] J. P. Perdew, K. Burke, and M. Ernzerhof, Phys. Rev. Lett. **77**, 3865 (1996).

[36] H. J. Monkhorst and J. D. Pack, Phys. Rev. B **13**, 5188 (1976).

[37] R. F. W. Bader, *Atoms in Molecules. A Quantum Theory* (Oxford University Press, New York, 1990).

[38] G. Henkelman, A. Arnaldsson, and H. Johnsson, Comput. Mater. Sci. **36**, 354 (2006).

[39] G. Henkelman and H. Jonsson, J. Chem. Phys. **113**, 9978 (2000).

[40] G. Henkelman, B. P. Uberuaga, and H. Jonsson, J. Chem. Phys. **113**, 9901 (2000).

[41] C. Cazorla, D. Alfè, and M. J. Gillan, Phys. Rev. B **77**, 224103 (2008).

[42] C. Cazorla, M. J. Gillan, S. Taioli, and D. Alfè, J. Chem. Phys. **126**, 194502 (2007).

[43] C. Cazorla, D. Errandonea, and E. Sola, Phys. Rev. B **80**, 064105 (2009).

[44] J. Cha, S. Lim, C. H. Choi, M.-H. Cha, and N. Park, Phys. Rev. Lett. **103**, 216102 (2009).

[45] Y. Ohk, Y.-H. Kim, and Y. Jung, Phys. Rev. Lett. **104**, 179601 (2010).

[46] K. E. Riley, M. Pitǒnak, J. Černy, and P. Hobza, J. Chem. Theory Comput. **6**, 66 (2010).

[47] Q. Wu and W. Yang, J. Chem. Phys. **116**, 515 (2002).

[48] C. S. Lin, R. Q. Zhang, S. T. Lee, M. Elstner, Th. Frauenheim, and L. J. Wan, J. Phys. Chem. B **109**, 14183 (2005).

[49] C. S. Lin, R. Q. Zhang, T. A. Niehaus, and Th. Frauenheim, J. Phys. Chem. C **111**, 4069 (2007).

[50] C. Feng, C. S. Lin, W. Fan, R. Q. Zhang, and M. A. Van Hove, J. Chem. Phys. **131**, 194702 (2009).

[51] R. C. Dunbar, J. Phys. Chem. A **104**, 8067 (2000).

[52] S. Mecozzi, A. P. West, Jr., and D. A. Dougherty, J. Am. Chem. Soc. **118**, 2307 (1996).

[53] J. C. Ma and D. A. Dougherty, Chem. Rev. **97**, 1303 (1997).

[54] S. R. Gadre and S. S. Pingale, J. Am. Chem. Soc. **120**, 7056 (1998).

[55] C. Møller and M. S. Plesset, Phys. Rev. **46**, 618 (1934).

[56] M. Head-Gordon, J. A. Pople, and M. J. Frisch, Chem. Phys. Lett. **153**, 503 (1988).

[57] R. Ditchfield, W. J. Hehre, and J. A. Pople, J. Chem. Phys. **54**, 724 (1971).

[58] V. A. Rassolov, M. A. Ratner, J. A. Pople, P. C. Redfern, and L. A. Curtiss, J. Comput. Chem. **22**, 976 (2001).

[59] GAUSSIAN 03, Revision D.02, M. J. Frisch *et al.*, Gaussian Inc., Wallingford CT, 2004.

[60] S. F. Boys and F. Bernardi, Mol. Phys. **19**, 553 (1970).

[61] S. Simon, M. Duran, and J. J. Dannenberg, J. Chem. Phys. **105**, 11024 (1996).

[62] S. L. Sun, C. S. Lin, R. Q. Zhang, C. S. Lee, and S. T. Lee, J. Phys. Chem. B **109**, 12868 (2005).

[63] Y. L. Zhao, C. S. Lin, R. Q. Zhang, and R. S. Wang, J. Chem. Phys. **122**, 194322 (2005).

[64] Y. Y. Sun, K. Lee, Y.-H. Kim, and S. B. Zhang, Appl. Phys. Lett. **95**, 033109 (2009).

[65] J. Ma, D. Alfè, A. Michaelides, and E. Wang, J. Chem. Phys. **130**, 154303 (2009).

[66] X. Dong, G. M. Wang, and E. Blaisten-Barojas, Phys. Rev. B **70**, 205409 (2004).

[67] M. S. Dresselhaus and G. Dresselhaus, Adv. Phys. **51**, 1 (2002).

[68] N. Emery, C. Herold, and P. Lagrange, J. Solid State Chem. **178**, 2947 (2005).

[69] L. W. Bruch, M. W. Cole, and E. Zaremba, *Physical Adsorption: Forces and Phenomena* (Oxford University Press, Oxford, 1997).

[70] M. C. Gordillo and J. Boronat, Phys. Rev. Lett. **102**, 085303 (2009).

[71] M. Calandra and F. Mauri, Phys. Rev. B **76**, 161406(R) (2007).

[72] C. Wood, N. Skipper, and M. Gillan, arXiv:1001.4923 (unpublished).

[73] M. Cobian and J. Íñiguez, J. Phys.: Condens. Matter **20**, 285212 (2008).

[74] G. Srinivas, C. A. Howard, S. M. Bennington, N. T. Skipper, and M. Ellerby, J. Mater. Chem. **19**, 5239 (2009).